Journal of Power Sources 220 (2012) 383–390

Contents lists available at SciVerse ScienceDirect

Journal of Power Sources

journal homepage: www.elsevier.com/locate/jpowsour

Numerical study on the cathode flooding of direct humidified proton exchange membrane fuel cell

Haruhiko Hirata [a,*], Soichiro Shimotori [b], Tsutomu Aoki [c]

[a] Plant Engineering Dept., Thermal & Hydro Power Systems & Services Div., Toshiba Corporation, 2-4, Suehiro-cho, Tsurumi-ku, Yokohama 230-0045, Japan
[b] Development, Toshiba Fuel Cell Power System Corporation, Japan
[c] Toshiba Fuel Cell Power System Corporation, Japan

HIGHLIGHTS

- Flooding characteristics for cathode GDL of direct humidified PEMFC.
- Co-flow and counter-flow of fuel and oxidant for pressure conditions of 1 and 3 atm.
- Numerical analysis results showed that flooding area was limited.

ARTICLE INFO

Article history:
Received 14 October 2011
Received in revised form
20 December 2011
Accepted 26 April 2012
Available online 5 May 2012

Keywords:
Proton exchange membrane fuel cell
Direct humidified cell
Flooding
Numerical analysis

ABSTRACT

In proton exchange membrane fuel cell (PEMFC) stack, the water management in the cell is required in order to ensure high cell performance. The water dry-out interferes with the proton migration in the electrode and electrolyte, and the water flooding interferes with the reactant gas transfer in the gas diffusion layer, consequently these phenomena affect the cell performance. One of the approaches to prevent the dry-out, a direct humidified cell with the channel to supply liquid phase water has been considered. In this cell configuration, sufficient water will be supplied to the anode, however the migrated water to the cathode from the anode shall be removed immediately in order to prevent the flooding. In this paper, numerical analysis that includes the behavior of the electrode reaction, heat transfer, gas flow, and evaporation and condensation of water was conducted regarding a direct humidified model cell. The co-flow and counter-flow of fuel and oxidant gases were considered for the pressure conditions of 1 atm and 3 atm. The water distribution in the vapor phase and liquid phase at the oxidant gas and cathode were calculated, and as a result of those, the flooding characteristics for each condition were evaluated.

1. Introduction

In proton exchange membrane fuel cell (PEMFC), it is well known that appropriate humidity in the cell is required in order to ensure high cell performance. The dry-out caused by low humidity interferes with the proton migration in the membrane electrolyte assembly (MEA), and the flooding caused by excessive humidity interferes with the reactant gas transfer in the gas diffusion layer (GDL). Therefore, studies regarding the liquid and vapor phase water management for the MEA, GDL, and gas channel have been conducted in these years.

For the purpose of evaluating the cathode channel flooding, numerous studies have been conducted. Shimpulee et al. [1] have conducted numerical study of the flooding in the GDL that includes a micro layer porous electrode using computational fluid dynamics (CFD) tool, and discussed about the cell performance reduction caused by various filling level of liquid water for the electrode pore. Le et al. [2] have conducted numerical study of the flooding in the gas channel and GDL using CFD tool, which includes the liquid phase water migration, and investigated the liquid water existence in the serpentine gas channels. Berg et al. [3] have conducted numerical study of the liquid and vapor phase water transfer characteristics in the cathode channel using one dimensional model of the co-flow and counter-flow for the fuel and oxidant. Cho et al. [4] have conducted coupling study of the experiment and CFD calculation, and estimated the flooding region with calculation based on the cell surface temperature that have been measured by experiment. Chen et al. [5] have conducted dynamic simulation study of the cell and humidifier, and calculated dynamic response of the vapor transfer in the membrane.

On the other hand, for the purpose of evaluating dry-out, Lister et al. [6] have conducted experimental study, and dry-out

* Corresponding author. Tel.: +81 45 500 1539; fax: +81 45 500 1594.
E-mail address: haruhiko.hirata@toshiba.co.jp (H. Hirata).

0378-7753/$ – see front matter © 2012 Published by Elsevier B.V.
doi:10.1016/j.jpowsour.2012.04.100

characteristics have been observed by measuring cell resistance with dry gas flow.

A direct humidified cell in which the liquid phase water is supplied has been considered for an approach to prevent the dry-out. In this cell configuration, the water channel that was contacted to the fuel channel will supply sufficient water to the anode GDL, and the dry-out will be prevented effectively. However, the migrated water to the cathode GDL and oxidant channel from the anode GDL shall be removed immediately by the evaporation with oxidant gas flow in order to prevent the flooding.

In this paper, numerical analysis that includes the behavior of the electrode reaction, heat transfer, gas flow, and evaporation and condensation of water was conducted regarding a direct humidified model cell. The co-flow and counter-flow of fuel and oxidant gases were considered for the pressure conditions of 1 atm and 3 atm. The flooding areas regarding each condition were estimated, and as a result of those the effect of flooding on the cell performance was evaluated.

2. Analysis method

The analysis features about the heat transfer and gas flow in the stack are the same as those of the code for MCFC [8], and the functions of the water evaporation and condensation have been added based on the code for PAFC [7], and function of the electrode reaction has been modified to simulate the PEMFC.

Regarding the electrode reaction, the following V–i characteristic equation [9] was adopted. This equation has been derived from the experiments of the single cell using 50.56 cm^2 "Nafion" membrane for the conditions of current density 54–323 mA cm^{-2}, temperature 323–358 K, hydrogen partial pressure 1.90–3.06 atm, and oxygen partial pressure 0.64–3.06 atm.

$$V = 1.229 - 0.85 \times 10^{-3} \times (T - 298.15) + 4.3085 \times 10^{-5} \times T \times \left[\ln\left(x_{H_2} \times x_{O_2}^{0.5}\right) + \ln\left(P^{1.5}\right)\right] - 0.9514 + 3.12 \times 10^{-3} \times T - 1.87 \times 10^{-4} \times T \times \ln(s \times i) + 7.4 \times 10^{-5} \times T \times \ln(c_{O_2}) - s \times i \times \left(0.01605 - 3.5 \times 10^{-5} \times T + 8.0 \times 10^{-5} \times s \times i\right) \quad (1)$$

Here, V is cell voltage V, T is temperature K, x is molar fraction, P is pressure atm, c is molar concentration mol cm^{-2}, s is cell area 50.56 cm^2, and i is current density A cm^{-2}.

The water evaporation and condensation rates were assumed to be infinite rates based on the saturated condition for the liquid phase water at the GDL and the vapor phase water at the oxidant gas.

The phosphoric acid evaporation and condensation rates in the PAFC had been calculated based on the activity energy change of the two components system consists of the water and phosphorous pentoxide, and the evaporation and condensation rates were derived with sufficient accuracy [7]. Where, the activity energy change was derived based on the vapor liquid equilibrium condition of the water and phosphorous pentoxide. Therefore, the water evaporation and condensation rates in this paper, in which the equilibrium condition were assumed, were also considered to have sufficient accuracy.

In addition to the above assumption, the following conditions were assumed.

(a) The anode GDL was assumed to be filled with sufficient water from the water channel.
(b) The amount of transferred water from anode to cathode by the drag of proton and diffusion was assumed to be 1.4 times the amount of composed by the electrode reaction.

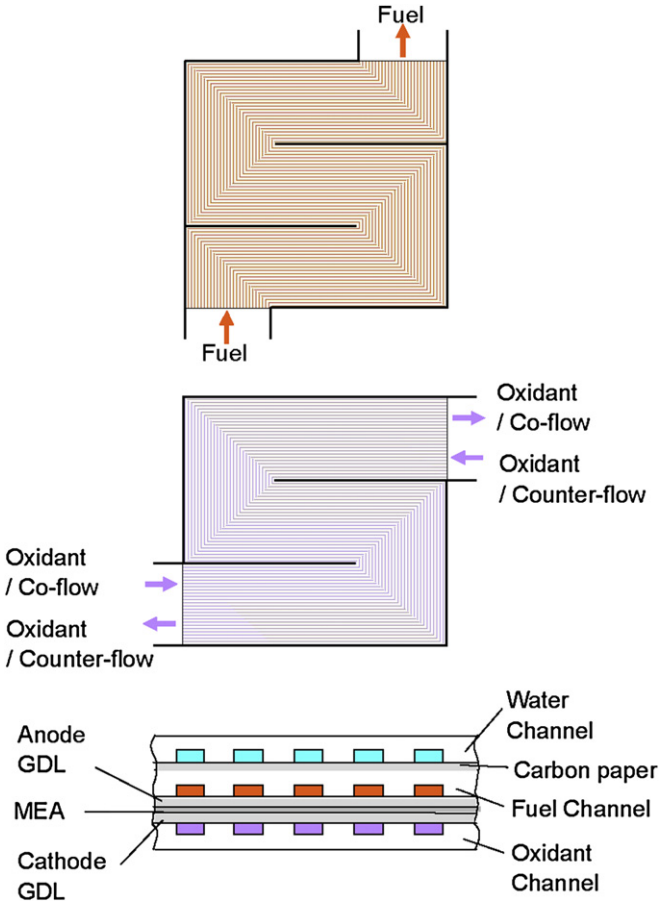

Fig. 1. Model cell configuration.

(c) The composed water at the cathode was assumed to be the liquid phase.
(d) The amount of evaporating water from the cathode GDL to oxidant gas was assumed to be less than or equal to the amount of water that was migrated from the anode GDL.

The assumption (b) was based on the results of the amount of migrated water from the anode to cathode by the drag of proton and diffusion, which was almost 1.4 times the composed water with the electrode reaction [10]. Where, it was derived regarding various current density conditions from 0.05 to 1.7 A cm^{-2} for conditions of 90 °C and 2 atm.

3. Analysis model and conditions

The outline of model cell is shown in Fig. 1, and specifications are shown in Table 1. The model cell consists of the anode GDL, MEA, cathode GDL, anode separator with fuel gas channel, cathode separator with oxidant gas channel, and the separator including

Table 1
Specifications for the model cell.

Cell size	170 × 170 mm
Separator thickness	1.5 mm
Channel width and height	1.0 × 0.5 mm
GDL thickness	0.3 mm
Separator thermal conductivity	139.6 W m^{-1} K^{-1} (in plane direction) 4.7 W m^{-1} K^{-1} (thickness direction)

water channel. The each separator has 18 serpentine channels that turn 2 times. In the case of co-flow configuration, the fuel, water, and oxidant were supplied at the left bottom corner and discharged at the right top corner in Fig. 1. In the case of counter-flow configuration, the fuel and water were supplied at the left bottom corner and discharged at the right top corner, and the oxidant was supplied at the right top corner and discharged at the left bottom corner in Fig. 1. The repeating thermal boundary condition that the water and oxidant separator surfaces had the same temperature and temperature gradient was adapted, as a result of this; the cell model represented a stack consists of infinity stacking cells. The adiabatic condition was adopted in each side of the cell. Analysis was conducted regarding the co-flow and counter-flow configurations for the pressure conditions of 1 and 3 atm.

The other conditions are shown in Table 2. Here, the current density condition of 350 mA cm^{-2} was selected to correspond with the equation (1). As the main purpose of this paper was to evaluate the effect of the water evaporation and condensation on the flooding area, a comparative study for such relatively low current density condition was attempted.

4. Analysis results

4.1. Cell voltage and cell average temperature

The cell voltage and cell average temperature for each analysis case are shown in Table 3. The cell voltage was increased about 7.7% and the cell average temperature decreased 1.8 K, according to the pressure increase from 1 atm to 3 atm for each gas flow configuration. The effect of the gas flow configurations on the cell voltage and cell average temperature was few.

4.2. Current density, cell temperature, water evaporation rate, and water evaporation margin

The current density distribution, cell temperature distribution, water evaporation rate distribution on cathode GDL, and water evaporation margin distribution on cathode GDL for the conditions of 1 atm and co-flow are shown in Figs. 2–5, respectively.

Here, net water evaporation or condensation rate was derived as infinite value based on the water equilibrium conditions as mentioned in Section 2. However, as a result of combination with the oxidant gas flow rate, the following apparent water evaporation rate was derived.

$$J_a = \frac{p_{H_2O}}{P} \times \frac{Q_O}{A} \quad (2)$$

Here, p_{H_2O} is saturated water vapor pressure atm, P is total pressure atm, Q_O is oxidant molar flow rate mol s^{-1}, A is cathode GDL area cm^2, and J_a is apparent water evaporation rate mol s^{-1} cm^{-2}. As shown in equation (2), the apparent water evaporation rate increased according to the oxidant gas flow rate increase, and decreased according to the total pressure increase.

The water evaporation margin on cathode GDL was defined as follows;

Table 2
Analysis conditions.

Pressure	1 atm, 3 atm
Gas inlet temperature	80 °C
Average current density	350 mA cm^{-2}
Fuel utilization (Dry H_2)	70%
Oxidant utilization (Dry air)	40%
Gas flow configuration	Co-flow, Counter-flow

Table 3
Analysis results.

Analysis conditions		Analysis results	
Pressure (atm)	Gas flow	Cell voltage (V)	Average cell temperature (K)
1.0	Co-flow	0.6813	358.1
1.0	Counter-flow	0.6814	358.2
3.0	Co-flow	0.7336	356.4
3.0	Counter-flow	0.7336	356.4

$$C_m = C_{c\to o} - C_{a\to c} \quad (3)$$

Here, C_m is water evaporation margin mol s^{-1} cm^{-2}, $C_{c\to o}$ is the amount of transferred water from the cathode GDL to oxidant gas mol s^{-1} cm^{-2}, and $C_{c\to o}$ is the amount of migrated water from the anode GDL to cathode GDL mol s^{-1} cm^{-2}. In the case of C_m is plus, the amount of migrated water from the anode to cathode will be fully transferred to the oxidant gas and the possibility of flooding will be low. On the other hand, in the case of C_m is minus, the amount of migrated water from the anode to cathode will not be fully transferred to the oxidant gas and the possibility of flooding will be high.

The current density was the largest at the inlet of oxidant and fuel, and it decreased 16% through the serpentine channel for the outlet of oxidant and fuel in Fig. 2. Here, the current density distribution was determined by equation (1) according to the pressure condition and the temperature distribution and molar fraction distributions of H_2 and O_2. The cell temperature was the lowest at the inlet of oxidant and fuel, and it increased 0.84% through the serpentine channel for the outlet of oxidant and fuel in Fig. 3, because the oxidant gas transferred the increased enthalpy by the electrode reaction from the oxidant inlet to the oxidant outlet.

The apparent water evaporation rate was the largest at the inlet of oxidant and fuel, and it decreased 18% through the serpentine channel for the outlet of oxidant and fuel in Fig. 4. The water partial

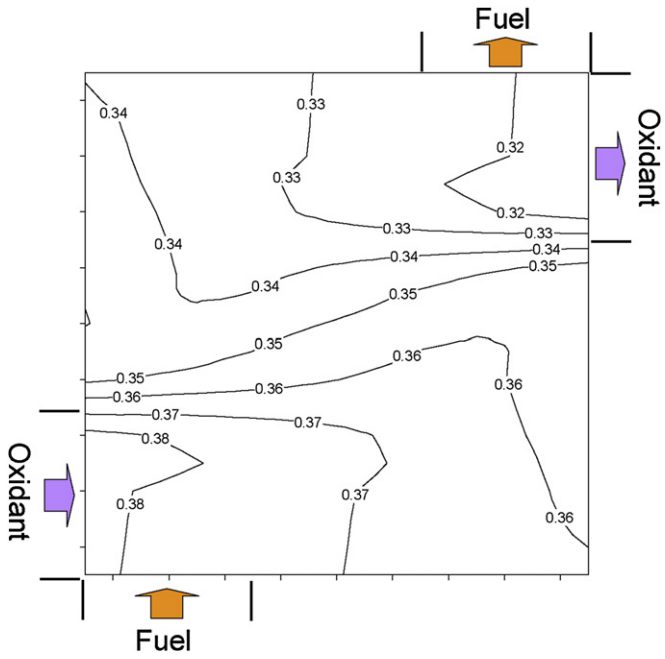

Fig. 2. Current density (A cm^{-2}), 1 atm, co-flow.

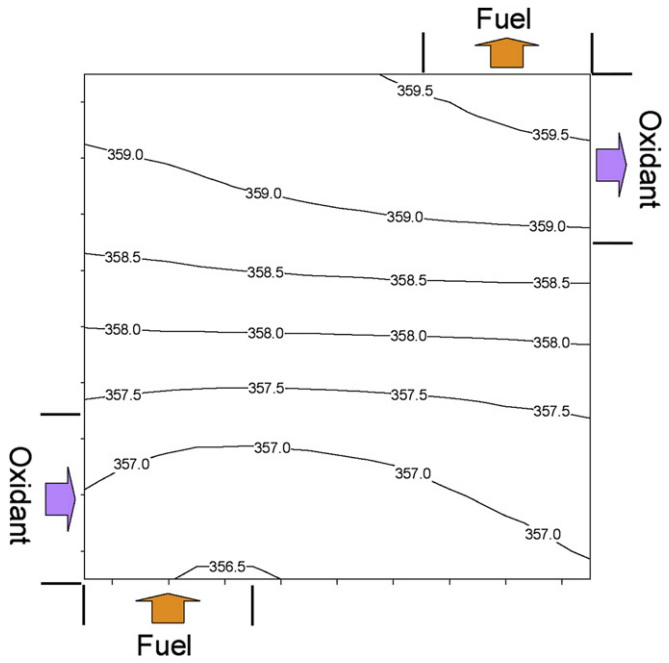

Fig. 3. Cell temperature (K), 1 atm, co-flow.

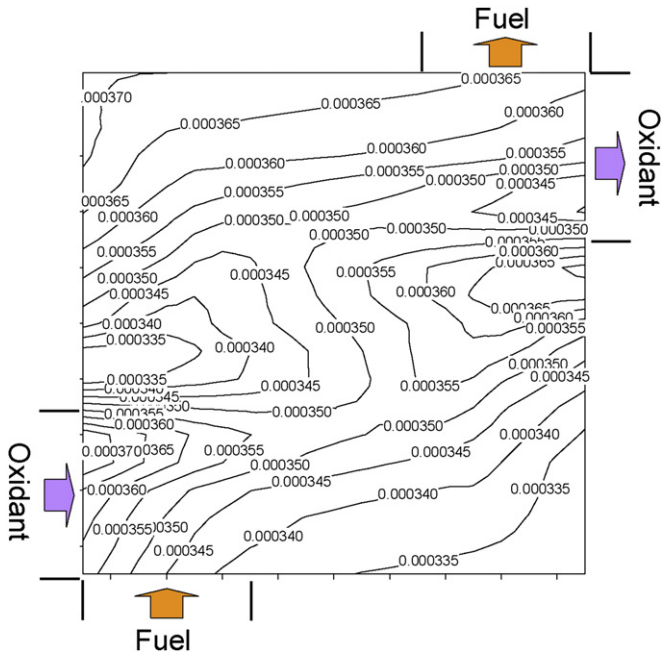

Fig. 5. H_2O evaporation margin (mol s^{-1} cm^{-2}), 1 atm, co-flow.

pressure in the oxidant gas was considered to be increased from the inlet to outlet of oxidant, thus the amount of transferred water from the cathode GDL to the oxidant gas was considered to be decreased through the serpentine channel for the outlet. The evaporation margin has plus value in the entire area of the cell in Fig. 5, and it was not considered that the flooding occurred.

The current density distribution, cell temperature distribution, water evaporation rate distribution on cathode GDL, and water evaporation margin distribution on cathode GDL for the conditions of 1 atm and counter-flow are shown in Figs. 6–9, respectively.

The current density was the largest at the oxidant inlet and fuel outlet, and it decreased 16% through the serpentine channel for the oxidant outlet and fuel inlet in Fig. 6. The cell temperature was the lowest at the oxidant inlet and fuel outlet, and it increased 0.70% through the serpentine channel for the oxidant outlet and fuel inlet in Fig. 7. The apparent water evaporation rate was the largest at the oxidant inlet and fuel outlet, and it decreased 18% through the serpentine channel for the oxidant outlet and fuel inlet in Fig. 8. The evaporation margin has plus value in the entire area of cathode GDL in Fig. 9, and it was not considered that the flooding occurred.

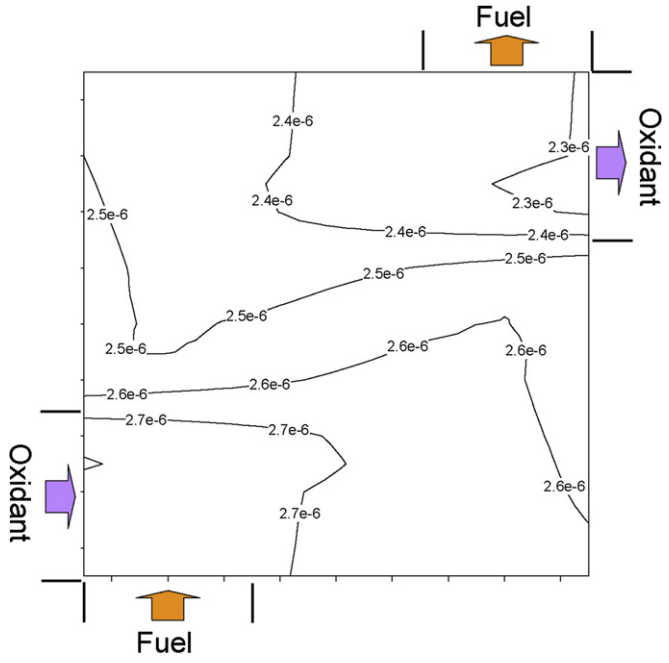

Fig. 4. Apparent H_2O evaporation rate (mol s^{-1} cm^{-2}), 1 atm, co-flow.

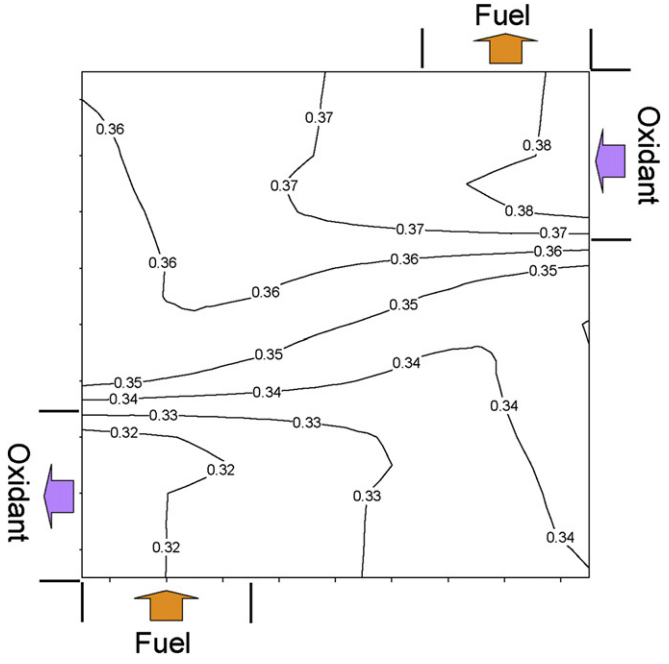

Fig. 6. Current density (A cm^{-2}), 1 atm, counter-flow.

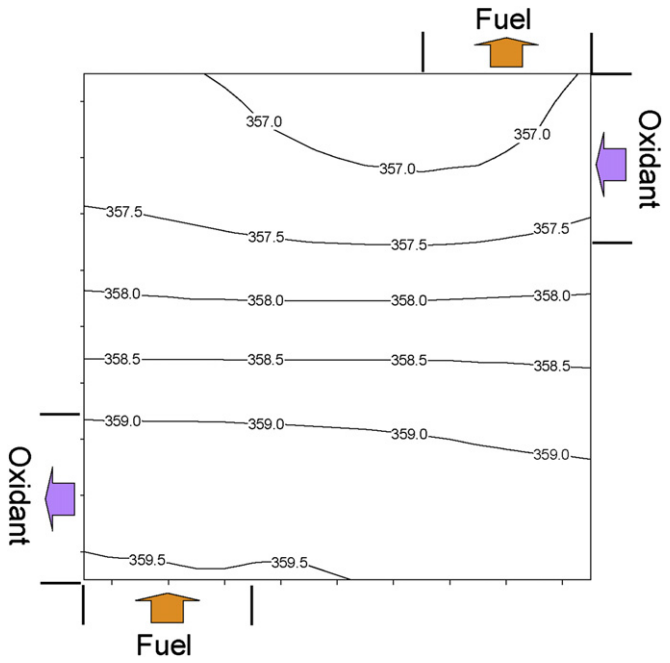

Fig. 7. Cell temperature (K), 1 atm, counter-flow.

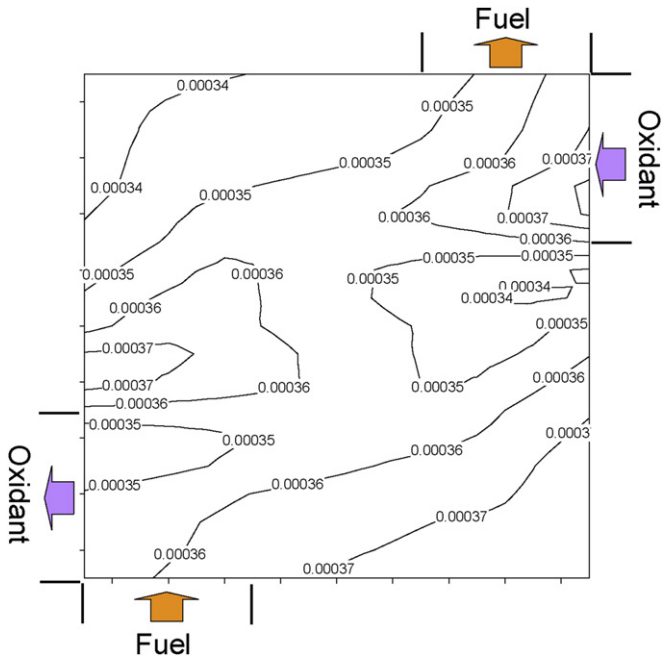

Fig. 9. H_2O evaporation margin (mol s^{-1} cm^{-2}), 1 atm, counter-flow.

The current density distribution, cell temperature distribution, water evaporation rate distribution on cathode GDL, and water evaporation margin distribution on cathode GDL for the conditions of 3 atm and co-flow are shown in Figs. 10–13, respectively.

The current density was the largest at the inlet of oxidant and fuel, and it decreased 16% through the serpentine channel for the outlet of oxidant and fuel in Fig. 10. Here, the current density distribution was similar with that for the pressure condition of 1 atm. The cell temperature was the lowest at the inlet of oxidant and fuel, and it increased 0.99% through the serpentine channel for the outlet of oxidant and fuel in Fig. 11. Here, the cell temperature distribution was lower about 1 K comparing with that for the pressure condition of 1 atm. The apparent water evaporation rate was lesser significantly at the outlet of oxidant and fuel comparing with that for 1 atm pressure condition, because the apparent water evaporation rate was decreased according to the increase of pressure as shown in equation (2). The evaporation margin was plus value in the most cathode GDL area except the outlet of oxidant and fuel. At the outlet of oxidant and fuel, the evaporation margin was minus value and it was considered that the flooding occurred.

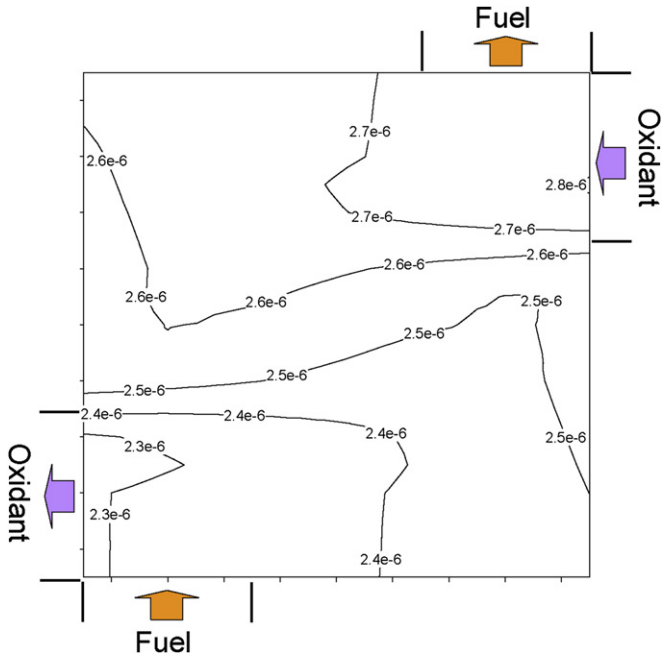

Fig. 8. Apparent H_2O evaporation rate (mol s^{-1} cm^{-2}), 1 atm, counter-flow.

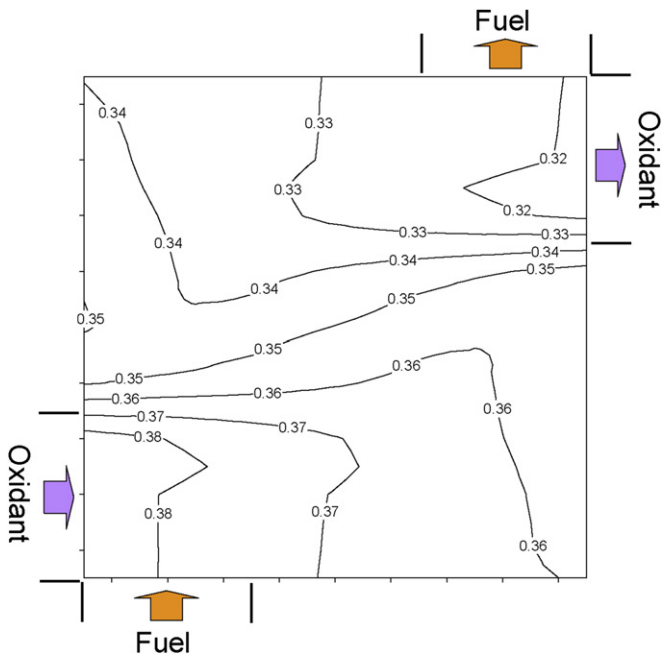

Fig. 10. Current density (A cm^{-2}), 3 atm, co-flow.

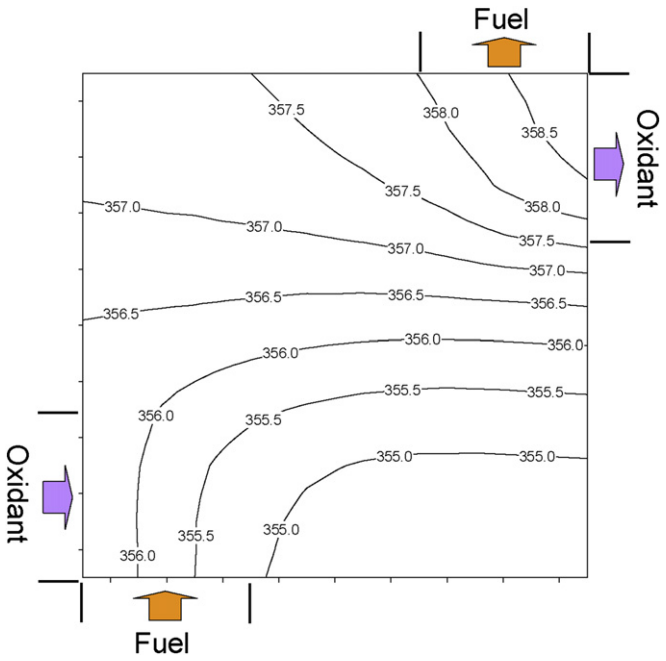

Fig. 11. Cell temperature (K), 3 atm, co-flow.

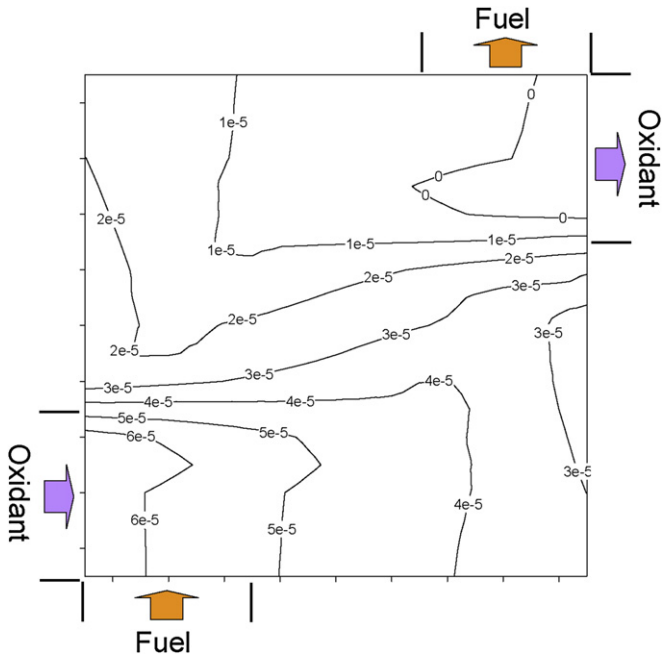

Fig. 13. H_2O evaporation margin (mol s^{-1} cm^{-2}), 3 atm, co-flow.

The flooding area corresponded with the area where the apparent water evaporation rate was less, the cell temperature was high, and the current density was less. Here, it was understood that the flooding was caused by the low apparent water evaporation rate. In addition, the flooding was considered to be effected by the water evaporation and condensation with oxidant gas flow, because the flooding was occurred at the area where the current density was low and the amount of migrated water from the anode to cathode was less.

The current density distribution, cell temperature distribution, water evaporation rate distribution on cathode GDL, and water evaporation margin distribution on cathode GDL for the condition of 3 atm and counter-flow are shown in Figs. 14–17, respectively.

The current density was the largest at the oxidant inlet and fuel outlet, and decreased 16% through the serpentine channel for the oxidant outlet and fuel inlet, and the current density distribution was similar with that for the case of 1 atm. The cell temperature was the lowest at the oxidant inlet and fuel outlet, and increased 0.99% through the serpentine channel for the oxidant outlet and

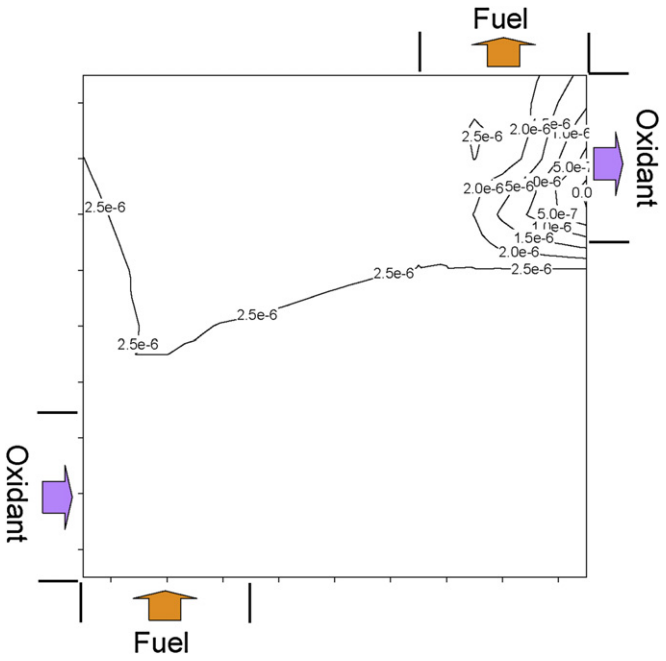

Fig. 12. Apparent H_2O evaporation rate (mol s^{-1} cm^{-2}), 3 atm, co-flow.

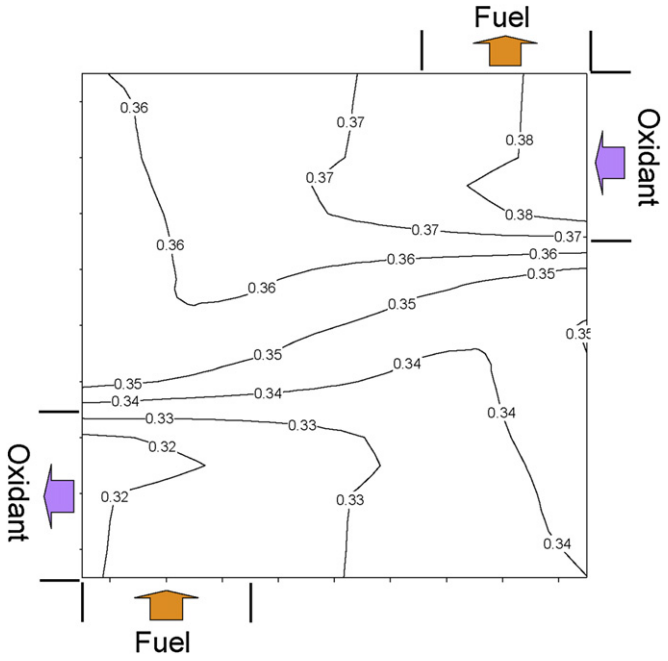

Fig. 14. Current density (A cm^{-2}), 3 atm, counter-flow.

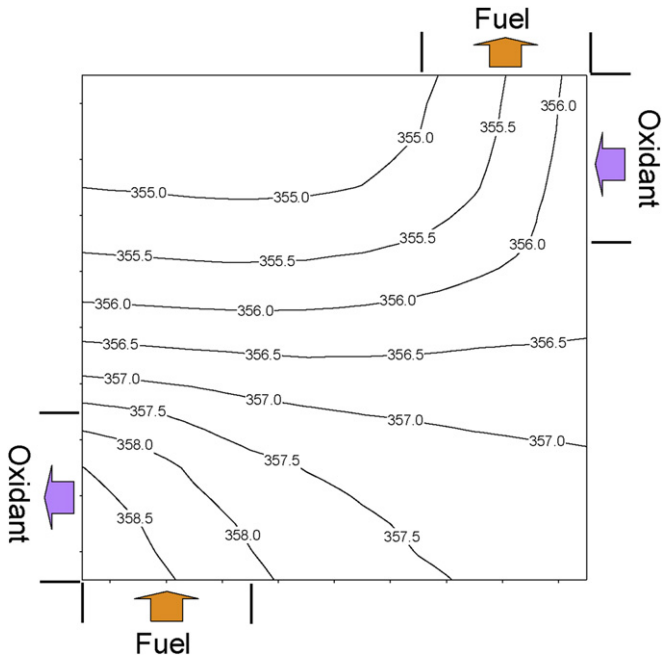

Fig. 15. Cell temperature (K), 3 atm, counter-flow.

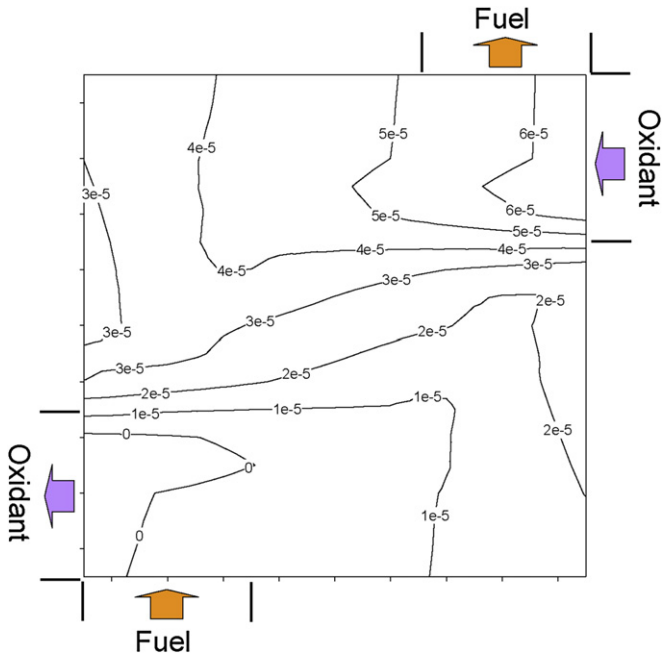

Fig. 17. H_2O evaporation margin (mol s^{-1} cm^{-2}), 3 atm, counter-flow.

fuel inlet. Here, the cell temperature distribution was lower about 1 K comparing with that for the pressure condition of 1 atm. The apparent water evaporation rate was lesser significantly at the oxidant outlet and fuel inlet comparing with that for 1 atm pressure condition. The evaporation margin was plus value in the most area of cathode GDL except the oxidant outlet and fuel inlet. At the oxidant outlet and fuel inlet, the evaporation margin was minus value and it was considered that the flooding occurred.

As similar results for the case of co-flow, the flooding area corresponded with the area where the apparent water evaporation rate was less, the cell temperature was high, and the current density was less.

The flooding areas for the co-flow and counter-flow of 3 atm pressure condition were limited at the oxidant outlet small areas, and the areas corresponded to the areas where the current densities were least. Therefore, the effect of flooding on the cell performance was not considered to be significant.

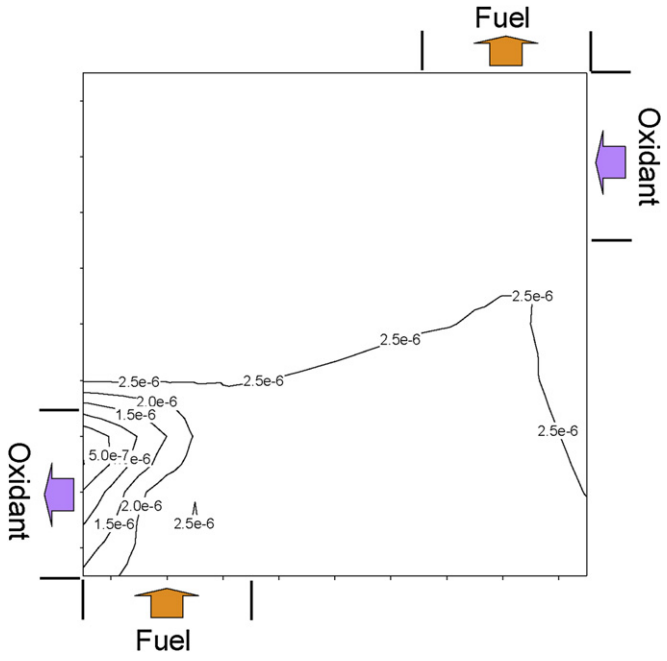

Fig. 16. Apparent H_2O evaporation rate (mol s^{-1} cm^{-2}), 3 atm, counter-flow.

5. Conclusion

The water migration from anode to cathode by electrode reaction, the water transfer by evaporation from cathode to oxidant gas with oxidant gas flow were calculated for a direct humidify model cell. The co-flow and counter-flow for the fuel and oxidant were considered for the pressure conditions of 1 atm and 3 atm, and as a result of those, the cathode flooding characteristics for each condition were evaluated.

In the case of pressure condition 1 atm, the water discharge by oxidant gas was conducted sufficiently and the flooding was not occurred for the co-flow and counter-flow.

In the case of pressure condition 3 atm, the water discharge by oxidant gas was prevented at the outlet of oxidant and the flooding was occurred for the co-flow and counter-flow both at the oxidant outlet. The flooding area corresponded with the area where the apparent water evaporation rate was less, cell temperature was high, and current density was less. In addition, the flooding was considered to be effected by the water evaporation and condensation with oxidant gas flow, because the flooding was occurred at the area where the current density was low and the amount of migrated water from the anode to cathode was less.

The flooding areas for the co-flow and counter-flow of 3 atm pressure condition were limited at the oxidant outlet small areas, and the areas corresponded to the areas where the current densities were least. Therefore, the effect of flooding on the cell performance was not considered to be significant.

List of symbols

V	cell voltage (V)
T	absolute temperature (K)
x	molar fraction
P	pressure (atm)
s	cell area (cm^2)
i	current density (A cm^{-2})
c	molar concentration
p_{H_2O}	saturated vapor pressure of water (atm)
Q_O	oxidant molar flow rate (mol s^{-1})
A	area (cm^2)
C_m	Evaporation margin (mol s^{-1} cm^{-2})
$C_{c\rightarrow o}$	H_2O transfer from cathode to oxidant (mol s^{-1} cm^{-2})
$C_{a\rightarrow c}$	H_2O transfer from anode to cathode (mol s^{-1} cm^{-2})

Subscripts

H_2	hydrogen
O_2	oxygen
H_2O	water

References

[1] S. Shimpalee, U. Beuscher, J.W. Van Zee, Electrochimica Acta 52 (24) (2007) 6748–6754.
[2] A.D. Le, B. Zhou, Journal of Power Sources 182 (2008) 197–222.
[3] P. Berg, K. Promislow, J. St. Pierre, J. Stumper, B. Wetton, Journal of the Electrochemical Society 151 (3) (2004) A341–A353.
[4] H.H. Cho Corfu Greece, in: 2nd WSEAS/ASME International Conference on Renewable Energy Sources (2008), pp. 21–28.
[5] D. Chen, H. Peng, Journal of Dynamic Systems, Measurement, and Control, Transactions ASME 127 (2005) 424–432.
[6] S. Lister, J.G. Santiago, Journal of Power Sources 188 (2009) 82–88.
[7] H. Hirata, T. Aoki, K. Nakajima, Journal of Power Sources 196 (2011) 8004–8011.
[8] H. Hirata, M. Hori, Journal of Power Sources 63 (1996) 115–120.
[9] J.C. Amphlett, R.M. Baumert, R.F. Mann, B.A. Pepply, P.R. Roberge, in: , Proceedings of 28th Intersociety Energy Conversion Engineering Conf, vol. 1, IECEC, Atlanta, 1993, pp. 1215–1220.
[10] T.V. Nguyen, R.E. White, Journal of Electrochemical Society 140 (8) (1993) 2178–2186.